Optical variability of the high synchrotron energy peaked blazar 1ES 1959+650 on various time-scales

You-Hong Zhang⋆ and Jia-Chen Li⋆

Department of Physics and Tsinghua Center for Astrophysics (THCA), Tsinghua University, Beijing 100084, China

ABSTRACT

We report the results of optical monitoring of the high synchrotron energy peaked blazar (HSP), 1ES 1959+650, performed with the 80-cm optical telescope at Xinglong Optical Observatory in 2010–2016. Our study was focused on the optical variability of the source on diverse time-scales over about 6 yr, which is helpful in understanding the variability mechanisms of blazars. Over 19 nights of intense photometric observations, we obtained 38 intranight light curves in the different bands. Intranight variability was not detected from all of these light curves. However, 1ES 1959+650 exhibited significant variations on the short-term (months) and long-term (years) time-scales. During the whole period of our monitoring, the maximum changes in the brightness of the source was 1.38 ± 0.05 and 1.17 ± 0.03 mag in the B and R waveband, respectively. The larger variability amplitude in the blue band than in the red one is demonstrated by the bluer-when-brighter spectral trend. The $B - R$ colour index showed a change of 0.21 ± 0.06 mag across our monitoring period. The non-detection of intranight variations of 1ES 1959+650 is in agreement with previous observations, showing that the optical fluxes of HSPs are less variable than those of intermediate/low synchrotron energy peaked blazars (ISPs/LSPs) on time-scales of hours. In contrast, the detections of significant short-term and long-term variability of the source suggest that the optical variability of HSPs might not be very different from those of ISPs/LSPs on time-scales of months and years. Finally, we discuss some possible scenarios for the differences and the similarities of optical variability on various time-scales between the two blazar subclasses.

Key words: galaxies: active – BL Lacertae objects: general – BL Lacertae objects: individual: 1ES 1959+650 – galaxies: photometry.

1 INTRODUCTION

Blazars include BL Lacertae (BL Lac) objects and flat spectrum radio quasars (FSRQs). They are well known for large amplitude and rapid flux variability across the whole electromagnetic wavelengths, high and variable radio and optical polarization, core-dominated radio morphology, and non-thermal emission (e.g. Ulrich, Maraschi & Urry 1997). The observational properties of blazars can be interpreted by the relativistically beaming effects which are believed to originate from the quite small viewing angles of the relativistic jets with respect to our line of sight (e.g. Urry & Padovani 1995). Because the beaming effects amplify the luminosity and shorten the times-scales, it is easier to detect the rapid flux variability of blazars compared to other active galactic nucleus (AGN) classes whose emission is not beamed to us. Therefore, blazars are ideal

targets to probe the central engine of AGNs by means of the flux variability study.

The spectral energy distributions (SEDs) of blazars can be well described by two broad spectral components which cover the electromagnetic spectrum from radio to gamma-ray wavelengths. Blazars are classified on the basis of the location of their SED peaks. Padovani & Giommi (1995) classified blazars into low energy peaked blazars (LBLs) and high energy peaked blazars (HBLs). The first SED component of LBLs peaks in the radio–optical wavelengths while the second component peaks in the GeV energies. For HBLs, the first SED component peaks in the UV–X-rays while the second component peaks in the TeV energies. Blazars are reclassified, based on the peak frequency (ν_{peak}) of synchrotron radiation, into low synchrotron energy peaked blazars (LSPs, $\nu_{peak} < 10^{14}$ Hz), intermediate synchrotron energy peaked blazars (ISPs, $10^{14} < \nu_{peak} < 10^{15}$ Hz) and high synchrotron energy peaked blazars (HSPs, $\nu_{peak} > 10^{15}$ Hz) (Abdo et al. 2010). Basically, LBLs include ISPs and LSPs, and HBLs are identical to HSPs.

Flux variability of blazars has been detected in most parts of the accessible electromagnetic spectrum, with variability time-scales ranging from minutes to years. In the literature, variability of blazars usually are investigated by classifying them into three broad classes (e.g. Gupta et al. 2016a,b), though such classifications are somewhat arbitrary and affected by the observational constraints in the different wavelengths. Flux changes, e.g. from hundredths to tenths of one magnitude in the optical band, over minutes to less than one day are called intraday variability (IDV, Wagner & Witzel 1995). Intranight variability and micro-variability, frequently used for characterizing optical variability of blazars, are identical to IDV (e.g. Gupta et al. 2016a). Brightness variations taking place from several days to few months are termed as short-term variability (STV). Finally, long-term variability (LTV) indicates flux variability occurring from several months to many years. In the latter two classes, variability of some blazars can reach up to several magnitudes in the optical bands (e.g. Villata et al. 2004).

Variability of blazars on various time-scales could be caused by different mechanisms. The detections of IDVs are important to understand the underlying physics of blazars. The instabilities and irregularities taking place in the smallest scales of blazar jets, perhaps originally arising from the accretion disc instabilities, are thought to be responsible for the IDVs in blazars (e.g. Gupta et al. 2016a,b). The jet structure on such small scales cannot be spatially resolved by current observational techniques (Lawrence 2016), even with the very long baseline radio interferometry (VLBI) in radio range. Thus, the detections and studies of blazar IDVs provide an alternative method to probe the fine structure of jets. Due to remarkable beaming effects, we need to obtain light curves of blazars with time resolution as high as possible.

Various studies have shown that the detections of blazar IDVs strongly depend on their SEDs. ISPs/LSPs show very high detection probability of IDVs in optical range (e.g. Cheng, Zhang & Xu 2013; Gupta & Joshi 2005; Zhai & Wei 2011, 2012), but not in X-rays (e.g. Liu & Zhang 2011; Gupta et al. 2016b). In contrast, for HSPs, IDVs can frequently be detected in X-rays (e.g. Zhang et al. 1999, 2002, 2005; Ravasio et al. 2004; Brinkmann et al. 2005;), but not in optical band (e.g. Gupta et al. 2016a). One possible interpretation for such a dependence is the differences of the synchrotron peak frequencies between ISPs/LSPs and HSPs. Since the optical and X-ray radiation is dominated by the highest energy electrons via synchrotron process and by the lower energy electrons through inverse Compton (IC) process, respectively, the ISP/LSP IDVs are expected to be more significant in the optical than in the X-ray band. Though the optical and X-ray emission of HSPs have synchrotron origins, the latter is dominated by the highest energy electrons while the former is controlled by the lower energy electrons. The X-ray IDVs are thus more remarkable than the optical IDVs for HSPs. The underlying physical process is that the higher energy electrons suffer faster cooling due to higher radiation power (Kirk & Mastichiadis 1999).

Interestingly, the optical IDVs in ISPs/LSPs show similar properties (e.g. the interband time lags and energy-dependent variability amplitude) to the X-ray IDVs in HSPs (e.g. Pian 2002; Zhang 2003; Cheng et al. 2013; Zhang et al. 2013; Zhang, Xu & Li 2016). A rational interpretation of such an analogue is that both the optical emission of ISPs/LSPs and the X-ray emission of HSPs are the highest energy tail of synchrotron radiation component. Both the optical IDVs in ISPs/LSPs and the X-ray IDVs in HSPs are thus controlled by the same physical process, i.e. the acceleration and cooling of the highest energy electrons responsible for the emission.

In order to study and compare the optical variability of ISPs/LSPs and HSPs on diverse time-scales, we have performed a project to observe a sample of blazars with the 80-cm optical telescope located at Xinglong Optical Observatory. Some results of this monitoring were presented in Cheng et al. (2013) for ON 231 and in Zhang et al. (2013, 2016) for BL Lac. These two objects are ISPs/LSPs.

In this paper, we present our optical observations for the HSP 1ES 1959+650. The observations were obtained over the time span of about 6 yr from 2010 to 2016. Our goal is to better understand the optical variability properties of the source on diverse time-scales. 1ES 1959+650 first was detected as an X-ray source (Elvis et al. 1992). It was then optically identified as a BL Lac object by Schachter et al. (1993) with redshift of 0.047. After the discovery of its very high energy gamma-ray emission (Nishiyama 1999), 1ES 1959+650 has been one of the most extensively monitored TeV targets, frequently coordinated with multiwavelength observations. It was highly variable in the X-ray and TeV energies on various time-scales (Giebels et al. 2002; Holder et al. 2003; Tagliaferri et al. 2003, 2008; Krawczynski et al. 2004; Gutierrez et al. 2006; Aliu et al. 2013, 2014; Kapanadze et al. 2016a,b). In the optical band, 1ES 1959+650 showed the LTVs of more than one magnitude (Gaur et al. 2012; Kapanadze & Janiashvili 2012; Sorcia et al. 2013), while the IDVs in the source have not been detected definitely yet (Gaur et al. 2012).

This paper is organized as follows. Section 2 describes the observations and data reduction. The variability analysis methods we used are given in Section 3. In Section 4, we present the results of variability analysis in detail. Section 5 is our discussion and conclusions.

2 OBSERVATIONS AND DATA REDUCTION

1ES 1959+650 was observed at Xinglong Optical Observatory of National Astronomical Observatories of Chinese Academy of Sciences (NAOC). Our observations were conducted with the 80-cm Tsinghua-NAOC Telescope (TNT), an equatorial-mounted $f/10$ Cassegrain optical telescope. The telescope is equipped with a Princeton Instrument thin back-illuminated CCD of 1340×1300 pixels. The pixel size is $\sim 20\,\mu$m. On the sky, the field of view of the CCD covers $\sim 11 \times 11$ arcmin^2. The CCD has read-out noise of 5 electrons Analog-to-Digital Unit (ADU)$^{-1}$ and its gain is 2.3 electrons ADU^{-1}.

The source was observed over the time span of about 6 yr from 2010 July to 2016 June. During 19 nights, we performed dense samplings to detect the optical IDVs in the source. During most of other nights, however, only one exposure per filter was done for the purpose to study the STVs and LTVs of 1ES 1959+650. We used standard Johnson–Cousin *BVRI* filters in turn. Several frames of flat-field and bias image were routinely taken during dusk and/or dawn during each night. The CCD was sufficiently cooled by liquid nitrogen, so we did not take dark frames during our observations.

We used MAXIM DL software to reduce the observation data and to perform aperture photometry for both 1ES 1959+650 and the standard stars. Each CCD frame was corrected by the bias frames and by the flat-field frames. We used Stars 4 and 6 as the standard stars in the source's field (Pace et al. 2013), since they are the closest stars to the source in both the brightness and position. Moreover, Pace et al. (2013) demonstrated that these stars are non-variable. They also provided the averaged magnitudes, on the basis of calibrations by different authors in the literature, for each standard star. Table 1 tabulates the magnitudes of Stars 4 and 6. With the differential photometric technique, we derived the apparent

Table 1. The standard stars used for the photometry of 1ES 1959+650 (from Pace et al. 2013).

Star	$B(\sigma)$	$V(\sigma)$	$R(\sigma)$	$I(\sigma)$
4	15.277(0.014)	14.501(0.008)	14.038(0.004)	13.619(0.004)
6	15.968(0.015)	15.204(0.012)	14.758(0.004)	14.365(0.004)

magnitudes of 1ES 1959+650 by averaging the magnitudes calibrated with the two stars. For the densely sampled nights, the photometric errors on the source are the standard deviations of the differential instrumental magnitudes between the two stars. For the nights with just one exposure, the photometric errors are the ones derived by the software. The apparent magnitudes and photometric errors of the source are tabulated in Table 2. For the nights with more than one exposure, the magnitudes are the ones averaged over the nights.

3 VARIABILITY ANALYSIS METHODS

In the literature, the differential photometry is the 'standard' method used to quantify the IDVs in blazars. We quantify the IDV analysis of 1ES 1959+650 by employing three different statistics (e.g. de Diego 2010), which are described below.

3.1 *C*-test

The *C*-test was introduced to quantify rapid variability of blazars by Romero, Cellone & Combi (1999). The variability detection parameters C_1 and C_2 with respect to Stars A and B, respectively, are defined as

$$C_1 = \frac{\sigma_A}{\sigma_{AB}} \tag{1}$$

$$C_2 = \frac{\sigma_B}{\sigma_{AB}}, \tag{2}$$

where σ_A, σ_B and σ_{AB} are the standard deviations of the differential instrumental magnitudes of the blazar and Star A, the blazar and Star B, and Star A and Star B, respectively. If $C_1 \geq 2.576$ and $C_2 \geq 2.576$, the variability of the source is claimed to be detected at the nominal confidence level of larger than 99 per cent.

3.2 *F*-test

The standard *F*-test is a normally distributed statistic which can be used to determine whether the variability of a source is significant

(de Diego 2010). The parameters of *F*-test, F_1 and F_2, are calculated with respect to Stars A and B, respectively,

$$F_1 = \frac{S_A}{S_{AB}} \tag{3}$$

$$F_2 = \frac{S_B}{S_{AB}}, \tag{4}$$

where S_A, S_B and S_{AB} are the variance of the differential instrumental magnitudes of the blazar and Star A, the blazar and Star B, and Star A and B, respectively. To quantify the significance of variability, the values of both F_1 and F_2 are compared with a critical value, $F_{\nu_Q, \nu_*}^{(\alpha)}$ (ν_Q and ν_* is the degree of freedom for the blazar and star light curve, respectively, and α is the significance level used to claim variability). We consider *F*-test with $\alpha = 1$ per cent and $\alpha = 0.1$ per cent which correspond to 2.6σ and 3σ significance level of variability, respectively. If the values of both F_1 and F_2 are larger than the critical value, the null hypothesis (i.e. no variability) is discarded.

3.3 ANOVA test

The one-way ANOVA test was applied by de Diego et al. (1998) to inspect the variability of quasars. We divided each light curve into k groups ($k = N/5$, N is the number of data points of the light curve) with each group having 5 data points. The variance of groups is defined as

$$S_G = 5 \sum_{j=1}^{k} (y_j - \bar{y})^2 / (k - 1), \tag{5}$$

where $\bar{y}$ is the average of the light curve and y_j is the average of the *j*th group. The variance of the light curve is

$$S_R = \sum_{j=1}^{k} \sum_{i=1}^{5} (y_{ij} - y_j)^2 / (N - k). \tag{6}$$

The ratio between these variances is

$$F = \frac{S_G}{S_R}. \tag{7}$$

The ratio, *F*, behaves like the *F*-statistic. To check the variability, we compare the value of *F* with the critical value, $F_{\nu_1, \nu_2}^{(\alpha)}$. As stated above, the degree of freedom is $\nu_1 = k - 1$ for each group and $\nu_2 = N - k$ for all groups. We then obtain $\nu_1 + \nu_2 = N - 1$, just corresponding to the degree of freedom for the original light curve. We performed *F*-test with $\alpha = 1$ per cent and $\alpha = 0.1$ per cent which corresponds to 2.6σ and 3σ significance level of claiming variability, respectively. We computed the *F*-value with respect to Stars A and B, and obtained F_1 and F_2, respectively. For a certain

Table 2. Excerpt of the photometric results of 1ES 1959+650. The full photometric data are available online.

Date (UT)	JD (2450000+)	N	$B(\sigma)$	$V(\sigma)$	$R(\sigma)$	$I(\sigma)$
2010-07-20	5398.234 749	62	15.913(0.019)	15.298(0.009)	14.816(0.012)	14.220(0.015)
2010-07-22	5400.121 476	4	15.992(0.040)	15.333(0.028)	14.825(0.031)	14.194(0.042)
2010-08-05	5414.222 880	56	15.841(0.028)	15.237(0.012)	14.770(0.014)	14.188(0.015)
2011-05-10	5692.336 726	2	...	15.041(0.036)	14.574(0.003)	...
2011-05-12	5694.339 730	1	...	15.096(0.056)	14.609(0.063)	...
2011-05-13	5695.332 121	1	...	15.060(0.023)	14.589(0.023)	...

Note. The first column indicates the UT date of the observation. The second column is the Julian Day (JD) of the middle time of the observations during the night. The third column (*N*) indicates the number of exposures per filter per night. The fourth–seventh columns are the apparent magnitudes in the *BVRI* bands, respectively. The magnitudes are averaged if more than one exposures are available during one night. The values in the parentheses indicate the photometric errors (see Section 2 for details).
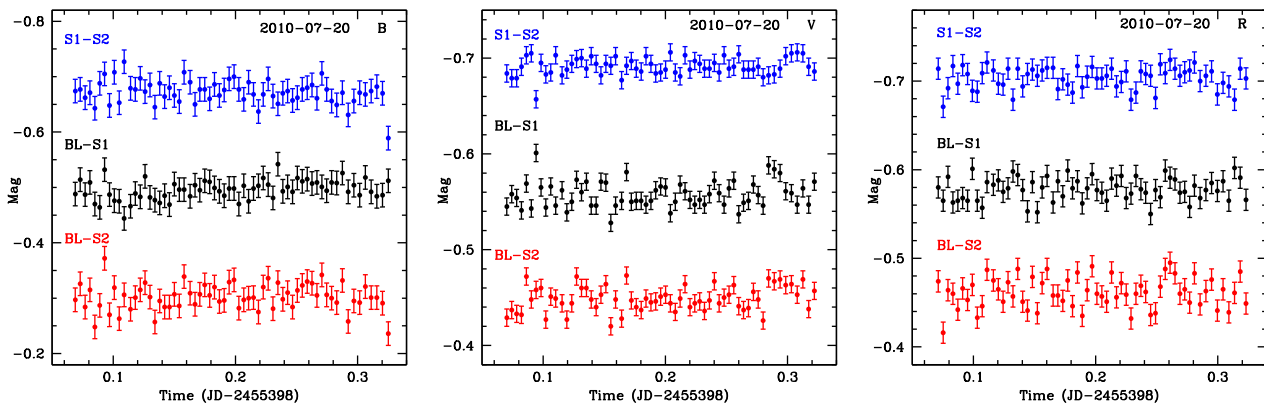
Figure 1. Excerpt of the differential light curves of 1ES 1959+650 obtained with TNT, showing intranight variability of the source. The observation dates and the filters are indicated in each plot. BL, S1 and S2 denote the source, Star 4 and 6, respectively. The blue light curves (S1− S2) present the differences of the instrumental magnitudes between the two standard stars. The black (BL −S1) and red (BL−S2) light curves show the differences of the instrumental magnitudes between the source and the two stars, respectively. For the visual convenience, the black and red light curves are shifted vertically. All of the differential light curves are available online.

significance level of α, if both F_1 and F_2 exceed the critical value, the null hypothesis (i.e. no variability) is rejected.

4 RESULTS

4.1 Intraday variability

We obtained 38 intensely sampled intranight light curves for 1ES 1959+650 during the 19 nights in 2010–2016. These light curves were gathered in the *BVRI* bands. In order of date and filter, Fig. 1 presents the differential light curves between the source and the two stars, showing the IDVs in the source with respect to Stars 4 and 6, respectively. This figure also plots the differential light curves between Stars 4 and 6, providing the changes of photometric condition during the nights. It appears that the source did not exhibit visible IDVs in any of the light curves, which is supported by the results derived from the variability analysis with the three test techniques described in Section 3. The parameters of these tests are tabulated in Table 3. It can be seen that these IDV light curves never exceed the tests at 99 per cent confidence level with these techniques simultaneously, suggesting that the IDVs were not detected in 1ES 1959+650 during our observing period. Our results are in agreement with those obtained by Gaur et al. (2012) with 45 IDV light curves in the *B* and *R* bands.

4.2 Short-term variability

In order to characterize the STVs of 1ES 1959+650, we separated our whole observations on the basis of its natural observational seasons. The observations in 2010 covered three nights only, so we do not discuss it in the sense of STV. Therefore, we obtained six STVs, which are plotted in Fig. 2 in time order. Each data point represents the apparent magnitude from one night. If more than one exposures were made during one night, the magnitudes were averaged. Among these STVs, the 2016 one covered about one month with seven data points only, but the other five ones lasted about 6–8 months with tens of data points. It appears that 1ES 1959+650 underwent two flares on time-scales of months in 2012 and 2013, respectively. Due to poor samplings and/or short time durations of the observations, it is unclear whether the source experienced flares in other four observational seasons. Nevertheless,

the source was variable during these seasons as shown by the STV light curves in Fig. 2.

Table 4 presents the magnitude ranges in the STVs. The variability amplitude of the six STVs ranges from ∼0.2–∼0.9 mag. Among these STVs, the largest amplitude of variability took place in 2012. Note that the magnitude ranges depend on the sampling rates and the time durations of the STVs. Table 4 also shows that the variability amplitude tends to increase with shorter wavelength.

4.3 Long-term variability

Fig. 3 is drawn using the nightly-averaged magnitudes from our observations performed in 2010–2016. Because the observations in the *V* and *I* bands were made in 2010–2012, only the *B* and *R* band light curves are presented for clarity. This figure provides a case to explore the LTV of 1ES 1959+650 in the optical band over time-scale of about 6 yr. It can been clearly seen that the source was variable. In particular, two highest brightness states were locally sampled in the 2012 and 2013 flares (see also Fig. 2).

On 2012 May 5, 1ES 1959+650 was in the brightest state with $B = 14.610 \pm 0.036$ mag and $R = 13.670 \pm 0.010$ mag. However, it came through the faintest states with indistinguishable brightness in two nights. On 2010 July 22, the source showed $B = 15.992 \pm 0.040$ mag and $R = 14.825 \pm 0.031$ mag. Similarly, it had $B = 15.936 \pm 0.034$ mag and $R = 14.839 \pm 0.028$ mag on 2014 August 4. During our observations of 6 yr, 1ES 1959+650 exhibited total changes of 1.382 ± 0.050 and 1.169 ± 0.030 mag in the *B* and *R* bands, respectively. The blue band variability amplitude is larger than the red band one.

4.4 Spectral variability

In Fig. 4, the $B − R$ and $V − R$ colour indices are plotted against the *R* magnitudes, respectively, to reveal the spectral variability of 1ES 1959+650 with its brightness. The errors on the $B − R$ and $V − R$ colour indices were propagated from the errors on the *B*, *V* and *R* magnitudes. Note that, compared to the $B − R$ colour indices, the number of the $V − R$ colour indices are much smaller because the observations in *V* band were conducted in 2010–2012 only. The bluer-when-brighter (BWB) trend of variability is pronounced for both the $B − R$ and $V − R$ colour indices,

Table 3. Results of intraday variability detections in 1ES 1959+650.

Date	Band	N	C-test C_1 C_2	F-test F_1 F_2 $F_c(0.99)$ $F_c(0.999)$	ANOVA F_1 F_2 $F_c(0.99)$ $F_c(0.999)$
2010-07-20	B	62	0.977 1.193	0.955 1.424 1.827 2.237	1.214 0.780 2.625 3.548
2010-07-20	V	62	1.486 1.422	2.209 2.023 1.827 2.237	0.684 0.992 2.625 3.548
2010-07-20	R	61	0.880 1.289	0.775 1.661 1.836 2.252	0.855 1.310 2.633 3.564
2010-07-20	I	61	1.048 1.160	1.098 1.346 1.836 2.252	1.465 0.929 2.633 3.564
2010-08-05	B	54	0.890 0.875	0.792 0.765 1.911 2.377	3.867 0.987 2.840 3.929
2010-08-05	V	56	1.238 1.104	1.532 1.220 1.888 2.338	1.832 0.855 2.743 3.760
2010-08-05	R	56	1.049 1.422	1.100 2.023 1.888 2.338	1.183 1.857 2.743 3.760
2010-08-05	I	55	1.066 1.207	1.136 1.457 1.899 2.357	1.735 1.092 2.754 3.781
2011-07-31	R	32	0.931 0.808	0.866 0.653 2.351 3.152	8.466 8.403 3.818 5.802
2011-08-01	R	34	0.845 0.774	0.714 0.599 2.287 3.036	4.396 0.942 3.754 5.656
2012-06-15	B	39	0.618 0.847	0.382 0.718 2.157 2.803	2.448 5.632 3.427 5.021
2012-06-15	R	39	1.145 1.321	1.311 1.744 2.157 2.803	1.916 2.145 3.427 5.021
2012-06-16	B	30	0.808 0.892	0.654 0.795 2.423 3.287	0.609 1.796 3.895 5.977
2012-06-16	R	32	0.446 0.911	0.199 0.829 2.351 3.152	0.331 1.874 3.818 5.802
2012-06-30	B	61	0.769 1.014	0.592 1.027 1.836 2.252	0.692 2.452 2.633 3.564
2012-06-30	R	61	0.828 1.054	0.685 1.110 1.836 2.252	0.924 0.356 2.633 3.564
2012-07-01	B	60	0.635 1.018	0.403 1.037 1.846 2.268	2.400 8.033 2.642 3.580
2012-07-01	R	41	0.817 1.057	0.668 1.118 2.114 2.727	0.939 4.123 3.238 4.675
2012-07-02	B	59	0.545 1.009	0.297 1.018 1.856 2.285	0.914 7.971 2.715 3.704
2012-07-02	R	58	0.602 1.093	0.363 1.194 1.866 2.302	1.673 4.714 2.724 3.722
2012-07-13	B	62	0.724 1.054	0.525 1.112 1.827 2.237	3.867 0.722 2.625 3.548
2012-07-13	R	63	0.826 1.057	0.682 1.117 1.818 2.222	1.199 1.555 2.617 3.532
2012-07-14	B	69	0.513 0.974	0.263 0.948 1.768 2.141	0.931 4.008 2.520 3.360
2012-07-14	R	68	0.790 1.148	0.625 1.318 1.776 2.153	3.760 5.795 2.526 3.373
2012-07-15	B	64	0.684 0.983	0.468 0.966 1.809 2.207	3.164 1.144 2.610 3.518
2012-07-15	R	64	0.735 1.111	0.540 1.235 1.809 2.207	2.167 1.409 2.610 3.518
2012-07-16	B	36	0.921 1.102	0.849 1.213 2.231 2.934	1.578 2.044 3.499 5.179
2012-07-16	R	38	0.634 1.029	0.402 1.059 2.181 2.844	2.024 1.965 3.449 5.070
2012-07-29	B	24	0.646 1.068	0.417 1.141 2.719 3.853	2.959 1.604 4.938 8.098
2012-07-29	R	22	0.778 1.284	0.605 1.649 2.857 4.127	3.615 8.152 5.092 8.487
2013-07-16	B	33	0.569 0.789	0.323 0.623 2.318 3.092	2.989 3.659 3.785 5.726
2013-07-16	R	26	0.757 0.895	0.573 0.800 2.604 3.629	3.537 3.625 4.369 6.947
2013-07-19	B	21	0.669 0.855	0.447 0.731 2.938 4.290	1.689 4.735 5.185 8.727
2013-07-19	R	23	0.774 0.889	0.599 0.791 2.785 3.983	3.091 19.296 5.010 8.280
2013-07-20	R	19	0.716 1.192	0.513 1.421 3.128 4.683	1.191 3.504 6.226 10.971
2014-08-14	R	38	0.389 1.085	0.151 1.178 2.181 2.844	6.124 9.739 3.449 5.070
2014-08-18	B	34	0.998 1.097	0.996 1.203 2.287 3.036	1.087 0.823 3.754 5.656
2014-08-18	R	34	0.977 0.949	0.954 0.901 2.287 3.036	3.873 4.736 3.754 5.656

indicating that the source showed larger variability amplitude with shorter frequency, as we obtained above. The $B - R$ colour index showed a change of 0.213 ± 0.058 mag across our monitoring period.

Table 5 presents the Pearson correlation coefficient (r) and the null hypothesis probability (p) of the correlations between the colour indices and magnitudes, indicating that the BWB spectral trends are indeed significant. We fitted the correlations with a linear function of the form $y = a \times x + c$ (y and x indicate the colour indices and magnitudes, respectively, while a and c are the slope and intercept of the function, respectively). The results of our fits are also presented in Table 5 and Fig. 4 (the solid lines). The positive slopes of the correlations between the colour indices and magnitudes suggest that 1ES 1959+650 exhibited the BWB spectral trend during the period of our observations.

5 DISCUSSION AND CONCLUSIONS

With the TNT observations in 2010–2016, we have studied the optical variability of 1ES 1959+650 on diverse time-scales. Our observations largely augmented the optical data base of the source,

one of the HSPs with a rather small amount of optical data compared to the classical blazars (mostly ISPs/LSPs).

The main reason of seldom monitoring the optical IDVs in HSPs may be due to the low duty cycles of micro-variability in the optical emission of these sources (e.g. Gupta et al. 2016a). We observed 1ES 1959+650 with relatively dense temporal resolutions and long durations during 19 nights, mainly in the B and R bands. No significant IDVs were detected during these nights. Gaur et al. (2012) also observed the same source during 24 nights from 2009 July to 2010 August and did not find any IDV either (see also Krawczynski et al. 2004). Therefore, the results of our IDV detections are in agreement with those of Gaur et al. (2012). Note that this conclusion was derived from the ground-based small aperture optical telescopes. Due to relatively poor photometric precession (usually a few hundredth of one magnitude), these telescopes might not be able to reveal the IDVs in HSPs. Nevertheless, even though the IDVs would exist in 1ES 1959+650 and/or other HSPs, the variability amplitude of these sources should be significantly smaller than those in ISPs/LSPs.

The detections of IDVs in HSPs may need much higher photometric precision than that achieved to date. As an example, the
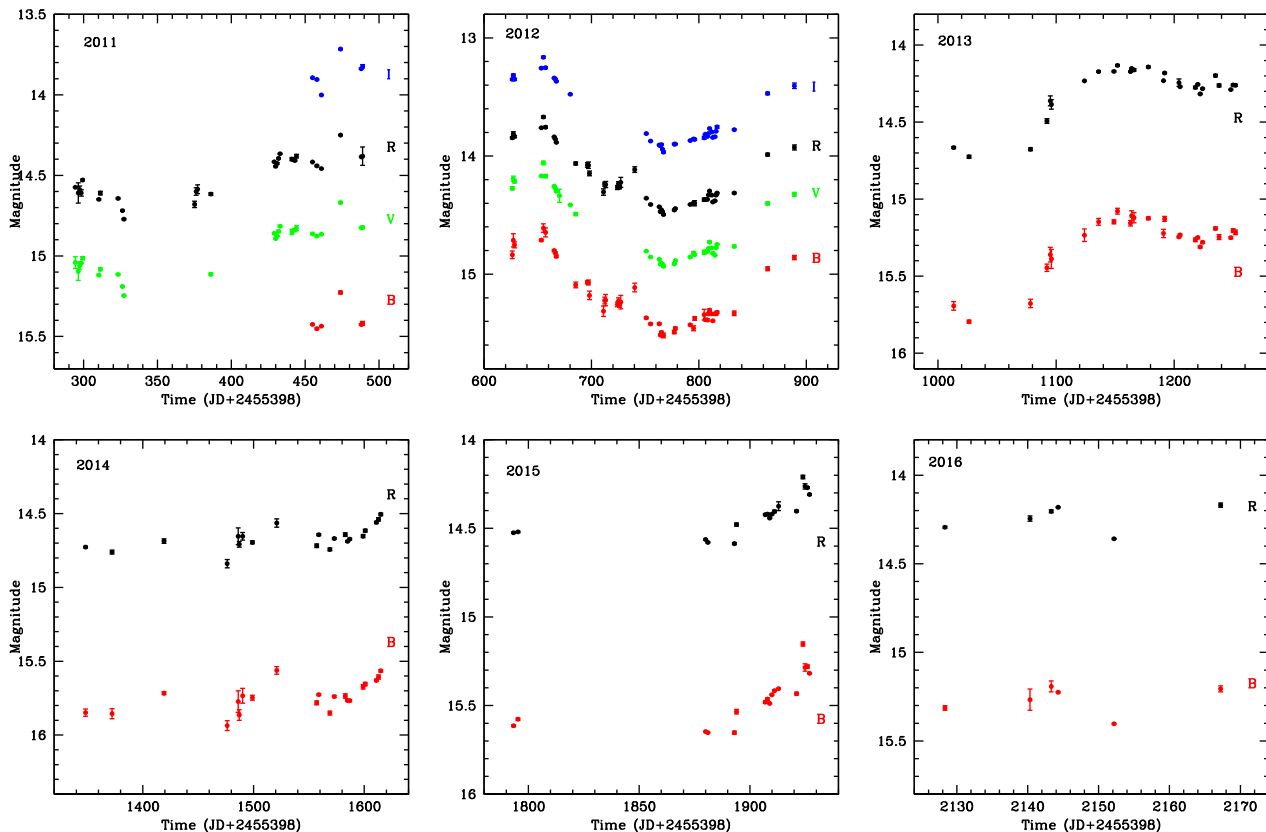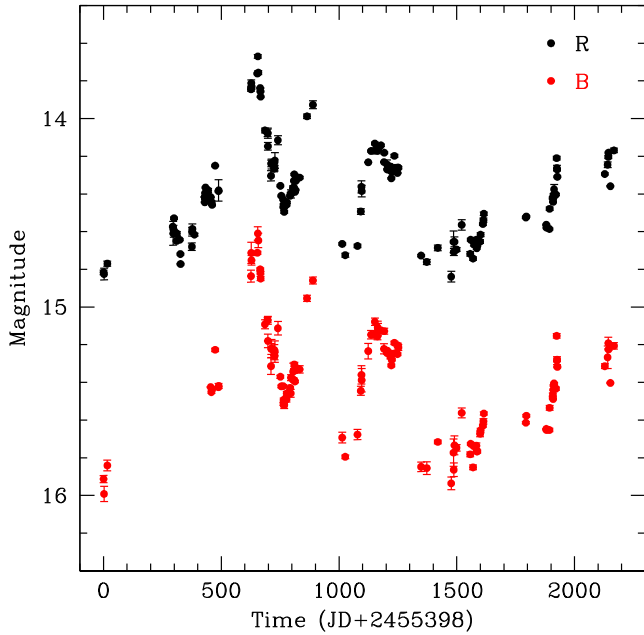
Figure 2. Short-term optical variability of 1ES 1959+650. The light curves are shown in time order of year on the basis of the natural seasons of observational visibility of the source. Each data point represents the data from one night. For the nights having more than one exposures, the magnitudes were averaged. The light curves in 2010 are not shown because they have just three data points in each band over about half a month.

Table 4. Magnitude ranges of short-term variability for 1ES 1959+650.

Period	Band	N	m_{max}	m_{min}	Δm
2010	B	3	15.992 ± 0.040	15.841 ± 0.028	0.151 ± 0.049
	V	3	15.333 ± 0.028	15.237 ± 0.012	0.096 ± 0.030
	R	3	14.825 ± 0.031	14.770 ± 0.014	0.055 ± 0.034
	I	3	14.220 ± 0.015	14.188 ± 0.015	0.032 ± 0.021
2011	B	6	15.452 ± 0.006	15.227 ± 0.009	0.225 ± 0.011
	V	26	15.246 ± 0.004	14.669 ± 0.006	0.577 ± 0.007
	R	29	14.772 ± 0.004	14.250 ± 0.004	0.522 ± 0.006
	I	6	14.001 ± 0.003	13.716 ± 0.004	0.285 ± 0.005
2012	B	46	15.519 ± 0.020	14.610 ± 0.036	0.909 ± 0.041
	V	36	14.933 ± 0.009	14.058 ± 0.015	0.875 ± 0.017
	R	47	14.495 ± 0.007	13.670 ± 0.010	0.825 ± 0.012
	I	35	13.967 ± 0.009	13.164 ± 0.009	0.803 ± 0.013
2013	B	27	15.795 ± 0.010	15.078 ± 0.019	0.717 ± 0.021
	R	27	14.725 ± 0.010	14.132 ± 0.006	0.593 ± 0.012
2014	B	21	15.936 ± 0.034	15.562 ± 0.026	0.374 ± 0.043
	R	21	14.839 ± 0.028	14.505 ± 0.009	0.334 ± 0.029
2015	B	17	15.653 ± 0.002	15.153 ± 0.012	0.500 ± 0.012
	R	17	14.586 ± 0.009	14.210 ± 0.010	0.376 ± 0.013
2016	B	6	15.403 ± 0.003	15.192 ± 0.031	0.211 ± 0.031
	R	6	14.359 ± 0.003	14.169 ± 0.012	0.190 ± 0.012

excellent photometric precision achieved by the *Kepler* mission (Borucki et al. 2010), used to find exoplanets by the transiting method, may be able to reveal the optical IDVs in HSPs. The very low duty cycles of the optical IDVs found in the HSPs so far might be artificial results, since the ground-based optical telescopes, usually used to detect the optical IDVs in blazars, have low photometric precision. Therefore, a more intrinsic reason for the differences of the optical IDVs between HSPs and ISPs/LSPs could be the amplitudes rather than the duty cycles of IDVs, i.e. the optical IDVs in HSPs might be significantly weaker than those in ISPs/LSPs. Future optical observations with high photometric precession may test this statement.
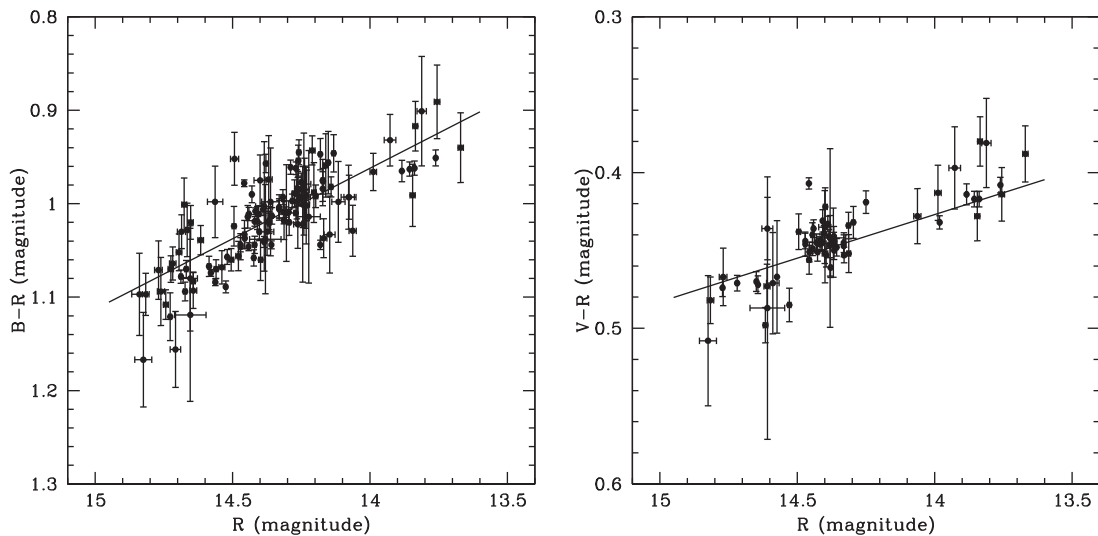
Figure 3. Long-term optical variability of 1ES 1959+650 in the *B* and *R* band during our observations of about 6 yr. Because the observations in *V* and *I* bands were done in 2010–2012 only, the light curves in the two bands are not shown for clarity.

However, 1ES 1959+650 exhibited genuine STVs and LTVs in the optical bands. The optical LTV, constructed using our observations in 2010–2016, was characterized by a large flare. The source showed significant variations by more than one magnitude and reached the maximum brightness in 2012. On the basis of the seasonal visibility, the STVs in 1ES 1959+650 were pronounced as well. The observations obtained by Gaur et al. (2012) supported the existence of optical STVs in the same source (see also Krawczynski et al. 2004; Sorcia et al. 2013). Our observations further revealed the presence of spectral variability correlated with brightness on long time-scales, in the sense that the source's optical spectra hardened when it brightened. The BWB spectral trend is in agreement

with the fact that the blue band showed larger amplitude of variability than the red band did. We suggest that the STVs and LTVs in 1ES 1959+650 could be similar to those in ISPs/LSPs (e.g. Villata et al. 2002 for BL Lac).

Variability of blazars were found to show different properties on diverse time-scales, which are thought to be caused by different physical mechanisms. The shock-in-jet model may interpret the fast variability (i.e. IDV or micro-variability) of blazars. When the shock propagates along the turbulent flow of plasma, it can accelerate the electrons to very high energy (e.g. Marscher & Gear 1985). The electrons are accelerated at the shock front. They are then cooled by synchrotron (and IC) process as they leave the shock front. The higher energy electrons cool faster than the lower energy ones do, so the radiation produced by the former comes from smaller volume compared to the radiation produced by the latter. Therefore, the emission produced by the higher energy electrons shows larger amplitude and shorter time-scale of variability than that produced by the lower energy electrons. Due to larger variability amplitude, the emission produced by the higher energy electrons may show higher duty cycle as well. 1ES 1959+650 frequently exhibited X-ray IDVs (Krawczynski et al. 2004; Kapanadze et al. 2016a,b), but its optical IDVs have not been detected yet (Gaur et al. 2012; this work). In particular, the fast X-ray variability of the source sometimes occurred on the time-scales as short as ∼1 ks (Kapanadze et al. 2016a,b). As one of the HSPs, the X-ray and optical emission of 1ES 1959+650 are thought to come from the same synchrotron component, but the electrons producing the X-ray emission have much higher energies than those producing the optical emission. Accordingly, the differences between the X-ray and optical IDVs in 1ES 1959+650 could be interpreted by the shock-in-jet model.

The X-ray fluxes of 1ES 1959+650 were highly variable on short and long time-scales. In another way, the X-ray STVs and LTVs were frequently detected in the source, which were accompanied mainly by the 'harder-when-brighter' (HWB) spectral trend (Giebels et al. 2002; Krawczynski et al. 2004; Kapanadze et al. 2016a,b). Similarly, the observations by Gaur et al. (2012) and us showed that the optical STVs and LTVs were often detected in 1ES 1959+650 as well. At the same time, the optical variability of the source on long time-scales exhibited similar spectral evolution, i.e. the BWB trend. Therefore,

Figure 4. Long-term spectral variability of 1ES 1959+650. Left plot shows the *B* − *R* colour indices versus the *R* magnitudes, and right plot shows the *V* − *R* colour indices versus the *R* magnitudes. The solid lines present the best linear fits to the data.

Table 5. Quantitative analysis of the correlations between the colour indices and magnitudes for 1ES 1959+650.

	r	p	a	c
$B - R$ versus R	0.707	2.404×10^{-20}	0.151 ± 0.014	-1.152 ± 0.195
$V - R$ versus R	0.703	6.524×10^{-11}	0.056 ± 0.007	-0.357 ± 0.102

Notes. r and p are the Pearson correlation coefficient and the null hypothesis probability of the correlation, respectively. a and c are the slope and intercept of the linear fit to the correlation in the form of $y = a \times x + c$ (y and x indicate the colour index and magnitude, respectively). The errors are at 1σ level.

even though the optical IDVs are different from the X-ray ones, the optical STVs and LTVs in 1ES 1959+650 can be similar to the X-ray ones. A possible explanation for the similar STVs and LTVs in the two bands is that the flux variability is caused by the variations of the Doppler factor of radiating blobs in the jets (e.g. Villata et al. 2002, 2004). The precession of an inhomogeneous helical jet, resulting in the changes of the viewing angle of the emitting blobs with respect to the line of sight, may be responsible for the changes of Doppler factor of the emitting blobs.

The BWB/HWB variability trend can be caused by different mechanisms (e.g. Gupta et al. 2016a). The non-thermal emission of blazars may consist of a variable and a stable component, with the former having a harder spectral slope than the latter. The stable component contributes to the underlying emission and the variable component is responsible for the increase of flux. The BWB/HWB trend is thus expected when a blazar brightens. One synchrotron emission component can also interpret the BWB/HWB trend. In this scenario, the flux increases are due to the re-injection of fresh electron population whose energy distribution is harder than that of the previously cooled one (Kirk & Mastichiadis 1999). The jet precession can change the Doppler factor of the received emission. If the emission has a 'convex' spectral shape, the variations of Doppler factor can cause the BWB/HWB trend as well (Villata et al. 2004).

Due to pronounced variability, the IDVs in ISPs/LSPs have been extensively observed in optical wavelengths, while the IDVs in HSPs have been well monitored in X-rays. Both the X-ray IDVs in HSPs and the optical IDVs in ISPs/LSPs show the high duty cycles of variability. Therefore, a more interesting investigation is to compare the properties of the optical IDVs in ISPs/LSPs to those of the X-ray IDVs in HSPs, rather than to compare the IDVs in HSPs and ISPs/LSPs in the same waveband, either in the optical or in the X-ray band. As we noted before, the temporal and spectral variations of HSPs in the X-ray band are similar to those of ISPs/LSPs in the optical band (e.g. Zhang 2010; Zhang et al. 2013, 2016). A number of studies showed that not only the X-ray variability amplitude of HSPs but also the optical variability amplitude of ISPs/LSPs tends to increase with increasing photon energy and that the spectra harden when the sources brighten (e.g. Brinkmann et al. 2005; Zhang et al. 2002, 2005, 2006, for the X-ray IDVs in HSPs, and Wu et al. 2005, 2012; Zhang et al. 2013, 2016, for the optical IDVs in ISPs/LSPs). Interband time lags were found in the X-ray IDVs of HSPs (e.g. Tanihata et al. 2001; Brinkmann et al. 2005) and in the optical IDVs of ISPs/LSPs (e.g. Papadakis et al. 2003; Wu et al. 2005; Cheng et al. 2013), respectively. More interestingly, the conversions between the soft and hard lags were already found in the X-ray IDVs of HSPs (e.g. Zhang 2002; Ravasio et al. 2004; Brinkmann et al. 2005, for Mrk 421; Zhang et al. 1999, 2002, 2006, for PKS 2155-304; see also Tanihata et al. 2001). An evidence for

this conversion was also detected in the optical IDVs of the classical ISP/LSP BL Lac (Zhang et al. 2013, 2016).

The SEDs of HSPs show higher synchrotron (and inverse Compton) peak energies than those of ISPs/LSPs, indicating that the intrinsic physical parameters of the emitting regions are systematically different between the subclasses of blazars. A number of SED modelling showed that HSPs have higher magnetic fields/electron energies and smaller sizes compared to ISPs/LSPs (e.g. Sambruna, Maraschi & Urry 1996). This determines that the cut-off energies of the synchrotron components are higher for HSPs than for ISPs/LSPs. The SEDs show that both the X-ray emission of HSPs and the optical emission of ISPs/LSPs are produced by the most energetic part of their respective electron energy distributions through the synchrotron process, suggesting that the same physical mechanisms can be responsible for the origin of the X-ray emission of HSPs and the optical emission of ISPs/HSPs. Similar IDV properties in many aspects are thus expected for the X-ray emission of HSPs and for the optical emission of ISPs/LSPs (Zhang et al. 2013, 2016). Since the X-ray emission of ISPs/LSPs comes from the lowest energy electrons through the IC process and the optical emission of HSPs are produced by the lower energy electrons through the synchrotron process, weaker variability are expected for both the X-ray IDVs in ISPs/LSPs and the optical IDVs in HSPs. As modelled by Kirk & Mastichiadis (1999), the variability pattern of a flare, such as time profile and interband time lag, is determined by the interplay between the electron acceleration time (t_{acc}) and cooling time (t_{cool}), and the flare duration (t_{var}). For the emission produced by lower energy electrons, since t_{acc} is always smaller than t_{cool}, t_{acc} will have much less effects on the properties of both the X-ray IDVs in ISPs/LSPs and the optical IDVs in HSPs. In contrast, for the X-ray emission of HSPs and the optical emission of ISPs/LSPs, both t_{acc} and t_{cool} can dominate the systems in different periods. Therefore, the interband hard and soft lags may occur in the X-ray IDVs of HSPs and in the optical IDVs of ISPs/LSPs (Zhang 2002).

The IDVs in blazars may be caused by the instabilities and/or irregularities of the smallest scales in the jets. These changes may originate from the accretion disc instabilities (Gupta et al. 2016a). Such small scales cannot be spatially resolved by current observational techniques. Thus, the observations of rapid flux variability of blazars are able to reveal information about the fine structure of the jets and accretion discs of blazars (Lawrence 2016). The relativistic beaming effects make the detections of the fast variability in blazars easier. In the future, high quality observations and detailed modelling of rapid variability will help us to better understand the changes of the smallest region in the jets and accretion discs of blazars.

ACKNOWLEDGEMENTS

REFERENCES

Abdo A. A. et al., 2010, ApJ, 716, 30
Aliu E. et al., 2013, ApJ, 775, 3

Aliu E. et al., 2014, ApJ, 797, 89
Borucki W. J. et al., 2010, Science, 327, 977
Brinkmann W., Papadakis I. E., Raeth C., Mimica P., Haberl F., 2005, A&A, 443, 397
Cheng X. L., Zhang Y. H., Xu L., 2013, MNRAS, 429, 2773
de Diego J. A., 2010, AJ, 139, 1269
de Diego J. A., Dultzin-Hacyan D., Ramirez A., Benitez E., 1998, ApJ, 501, 69
Elvis M., Plummer D., Schachter J., Fabiano G., 1992, ApJS, 80, 257
Gaur H. et al., 2012, MNRAS, 420, 3147
Giebels B. et al., 2002, ApJ, 571, 763
Gupta A. C., Joshi U. C., 2005, A&A, 440, 855
Gupta A. C. et al., 2016a, MNRAS, 458, 1127
Gupta A. C., Kalita N., Gaur H., Duorah K., 2016b, MNRAS, 462, 1508
Gutierrez K. et al., 2006, ApJ, 644, 742
Holder J. et al., 2003, ApJ, 583, L9
Kapanadze B. Z., Janiashvili E., 2012, Ap&SS, 339, 339
Kapanadze B., Romano P., Vercellone S., Kapanadze S., Mdzinarishvili T., Kharshiladze G., 2016a, MNRAS, 457, 704
Kapanadze B., Dorner D., Vercellone S., Romano P., Kapanadze S., Mdzinarishvili T., 2016b, MNRAS, 461, L26
Kirk J. G., Mastichiadis A., 1999, Astropart. Phys., 11, 45
Krawczynski H. et al., 2004, ApJ, 601, 151
Lawrence A., 2016, in Mickaelian A., Lawrence A., Magakian T. Y., eds, ASP Conf. Series Vol. 505, Astronomical Surveys and Big Data. Astron. Soc. Pac., San Francisco, p. 109
Liu L., Zhang Y. H., 2011, JApA, 32, 173
Marscher A. P., Gear W. K., 1985, ApJ, 298, 114
Nishiyama T., 1999, in Kieda D., Salamon M., Dingus B., eds, Proc. 26th Int. Cosmic Ray Conf. Vol. 3, Under the auspices of the International Union of Pure and Applied Physics (IUPAP). Univ. Utah, Salt Lake City, p. 370
Pace C. J., Pearson R. L., Ward Moody J., Joner M. D., Little B., 2013, PASP, 125, 344
Padovani P., Giommi P., 1995, MNRAS, 277, 1477
Papadakis I. E., Boumis P., Samaritakis V., Papamastorakis J., 2003, A&A, 397, 565
Pian E., 2002, Publ. Astron. Soc. Aust., 19, 49
Ravasio M., Tagliaferri G., Ghisellini G., Tavecchio F., 2004, A&A, 424, 841
Romero G. E., Cellone S. A., Combi J. A., 1999, A&AS, 135, 477
Sambruna R. M., Maraschi L., Urry C. M., 1996, ApJ, 463, 444
Schachter J. F. et al., 1993, ApJ, 412, 541
Sorcia M. et al., 2013, ApJS, 206, 11

Tagliaferri G., Ravasio M., Ghisellini G., Tavecchio F., Giommi P., Massaro E., Nesci R., Tosti G., 2003, A&A, 412, 711
Tagliaferri G. et al., 2008, ApJ, 679, 1029
Tanihata C., Urry C. M., Takahashi T., Kataoka J., Wagner S. J., Madejski G. M., Tashiro M., Kouda M., 2001, ApJ, 563, 569
Ulrich M.-H., Maraschi L., Urry C. M., 1997, ARA&A, 35, 445
Urry C. M., Padovani P., 1995, PASP, 107, 803
Villata M. et al., 2002, A&A, 390, 407
Villata M. et al., 2004, A&A, 421, 103
Wagner S. J., Witzel A., 1995, ARA&A, 33, 163
Wu J. H., Peng B., Zhou X., Ma J., Jiang Z. J., Chen J. S., 2005, AJ, 129, 1818
Wu J. H., Böttcher M., Zhou X., He X. T., Ma J., Jiang Z. J., 2012, AJ, 143, 108
Zhai M., Wei J. Y., 2011, A&A, 531, A90
Zhai M., Wei J. Y., 2012, A&A, 538, A125
Zhang Y. H., 2002, MNRAS, 337, 609
Zhang Y. H., 2003, Publ. Yunnan Observatory, 93, 26
Zhang Y. H., 2010, ApJ, 713, 180
Zhang Y. H. et al., 1999, ApJ, 527, 719
Zhang Y. H. et al., 2002, ApJ, 572, 762
Zhang Y. H., Treves A., Celotti A., Qin Y. P., Bai J. M., 2005, ApJ, 629, 686
Zhang Y. H., Treves A., Maraschi L., Bai J. M., Liu F. K., 2006, ApJ, 637, 699
Zhang Y. H., Bian F. Y., Li J. Z., Shang R. C., 2013, MNRAS, 432, 1189
Zhang Y. H., Xu L., Li J. C., 2016, AN, 337, 286

SUPPORTING INFORMATION

Supplementary data are available at *MNRAS* online.

Table 2. The photometric results of 1ES 1959+650. The first column indicates the UT date of the observation.
Figure 1. The differential light curves of 1ES 1959+650 obtained with TNT, showing intranight variability of the source.

Please note: Oxford University Press is not responsible for the content or functionality of any supporting materials supplied by the authors. Any queries (other than missing material) should be directed to the corresponding author for the article.

This paper has been typeset from a TEX/LATEX file prepared by the author.